CHAPTER 5
FLAT-ROLL TWO-ROLL MILLING EXPERIMENTS

This chapter outlines a series of two-roll milling experiments using variety Q96 prepared sugar cane and final bagasse from Invicta sugar-mill. Time series of digital images were captured for all experiments, forming the basis for numerical image analysis. The experiment involved eight prepared cane and eight final bagasse experiments, providing local fibre deformation data over a wide range of compaction, for the case of roughened flat–surfaced rolls. Significant limitations associated with the rolling apparatus were identified during the trials. Failure to obtain a quality mate between the viewing window and the samples caused problems for the prepared cane experiments, as a juice film over the viewing area was not always obtained. Instead, the juice extracted from the blanket formed a moving front that resulted in poor fibre displacement measurement. However, small sections of the footage captured for the prepared cane experiments were identified as suitable for steady–state ITA analysis.
The final bagasse experiments were not influenced by this juice front problem, due to the low moisture content of this material. The eight final bagasse tests were analysed using the ITA direct software for a slice of material in the centre section of each sample. The deformation results showed strong qualitative trends in the measured fields of deformation across the set of experiments. However, quantitatively the results varied significantly due to poor control of the mill roll speeds.

5.1 Aims and scope of the experimental program

The aims of the experimental program were:

1. Collect visual data for image measurement analysis.
2. Determine optimal ITA mesh density for analysis of prepared cane and bagasse at the scale of experimentation.
3. Measure the 2D local fibre deformation field for each material sample.
4. Assess the homogeneity of prepared cane and bagasse under two-roll milling conditions.

Experimental program scope:

1. All prepared cane experiments were conducted using one variety of cane. Only fresh prepared cane of one preparation level was used.
2. All final bagasse experiments were conducted using material from the same sample of bagasse taken from Invicta mill.
3. Image data was collected for all experiments.
4. Juice extraction was given no consideration.

5.2 Apparatus

Cane was prepared in the SRI rotary hammer shredder at the Sugar Research Institute (SRI). The rolls used for the two-roll experiments were cast iron with a width of 230 mm and a diameter of 750 mm. A steel non-porous side plate was used on one side of the rolls and the footage was captured through a non-porous glass 'viewing window' on the other side of the rolls. The flat rolls employed for all tests were also non–porous and were roughened using 60 grit emery tape on the roll surfaces. The viewing sides of the rolls were painted a non-reflective black to eliminate reflection from the apparatus. The rolls are shown in Figure 5.1.

Figure 5.1. Flat rolls employed for the two-roll milling trials.

The tests were performed in the C. R. Murry experimental milling facility at James Cook University (Figure 5.2(a)). The experimental mill is equipped with two counter-rotating rolls that are powered with hydraulic drives. Bagasse blankets are fed into the mill rolls with a live belt feeder as shown in Figure 5.2(b).

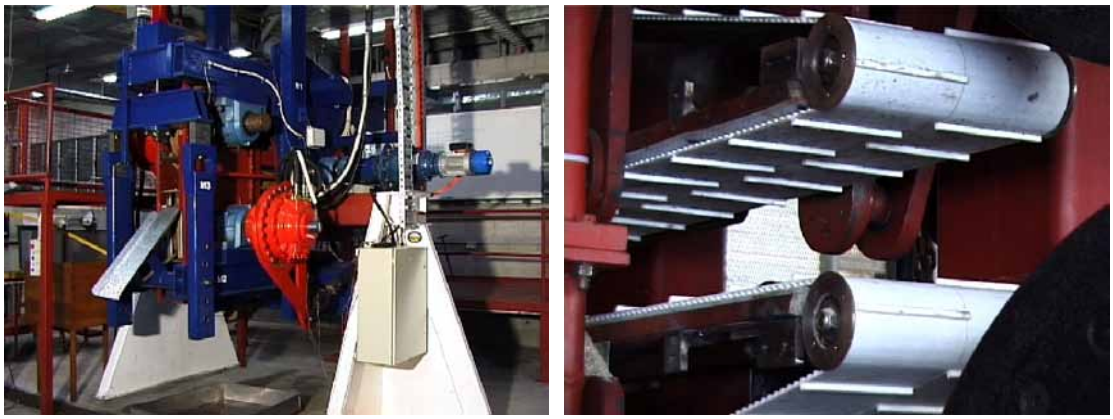

(a) (b)

Figure 5.2. a) C. R. Murry advanced experimental milling facility, b) Mill live belt feeder.

The CCD unit (Sony DCR-TRV900) was mounted on a two–dimensional traversing system that was designed specifically for collecting imagery from the experimental mill. The CCD unit was set as far from the viewing plane as possible in order to achieve a telescopic focal plane for image capture. The CCD was connected to an Apple I-mac Computer via an IEEE 1394 connection. This arrangement is shown in Figure 5.3.

Figure 5.3. CCD traversing system and image acquisition apparatus.

A light shroud was erected around the CCD and MTS machine in order to eliminate reflections from the surroundings. A 2000 Watt studio photographic light mounted on a tripod illuminated the samples. The camera shroud and studio light are shown in Figure 5.4.

Figure 5.4. The camera, light shroud and studio light employed for the experiments.

5.3 Procedure

The cane used in the experiment was variety Q96 grown in the Mackay region. Cane stalks were cut, cleaned and prepared in the SRI hammer shredder at 2000 revolutions per minute at the SRI in Mackay. A portion of the cane was thoroughly mixed (Anon. 1991) and two 500 gram samples were taken by SRI staff for fibre content analysis. The prepared cane was loaded into containers and promptly delivered in a refrigerated vehicle to the milling laboratory and stored in a cold room at -4°C. All experiments were conducted within 14 hours of the cane being stored. The average mass fraction fibre content of the cane was reported to be 13.1%. Final bagasse was collected from the last mill on A-side milling train at Invicta mill and stored at -4°C. All bagasse tests were conducted using this material. The bagasse was thoroughly mixed (Anon. 1991) and two 200 gram samples were taken for fibre content determination. The results of the fibre tests are shown below in Table 5.1.

Sample #	1	2
Initial can mass [g]	1312.2	1300.7
Initial bagasse mass [g]	200	200
Mass out 1 [g]	1424.6	1413.6
Mass out 2 [g]	1424.5	1413.6
Mass of hot dry can [g]	1320.2	1308.7
Fibre mass [g]	104.3	104.9
Fibre content	0.521	0.525
Average fibre content	0.523	

Table 5.1. Mass fraction fibre content analysis for the final bagasse.

Material seed was prepared by sieving fifteen kilograms of bagasse through a sieve stack containing three sieve sizes (11 mm, 7 mm, 2.5 mm). The material from the 2.5 mm aperture sieve was dyed black and dried. One hundred grams of material seed was mixed with one–quarter of each experimental sample prior to sample loading and pre–compression. The material seed is shown below in Figure 5.5.

Figure 5.5. Material seed for enhancing contrast in experimental samples.

Material samples were loaded into the pre–compression apparatus as evenly as possible in order to achieve an even void distribution. The material containing the seed was placed into the viewing window side of the pre–compressor. A pre-compressive load of 20 tonnes was applied to the samples in order to prepare the samples for processing in the two-roll mill. The pre-compressor is shown in Figure 5.6.

Figure 5.6. Pre-compressor used to prepare blankets for processing.

Each sample was then placed into the live feeder on the experimental mill. The rolls were started and allowed to settle at the desired surface speed and the blankets were fed through the two counter-rotating rolls. Roll load and torque traces for both the top and bottom rolls were recorded and stored in Microsoft Excel data files for analysis.

5.4 Apparatus limitations

The experimental mill is a powerful machine that is capable of reproducing factory crushing rates and nip compactions. The experimental procedures associated with the apparatus are well defined and are suitable for industrial experimentation. However, the apparatus poses significant limitations for precise image measurement of material deformations. These limitations can be categorised under three major causes: the pre–compressor, the roll fluid drives and mill structure.

5.4.1 The pre–compressor

There were three major limitations imposed by the sample pre–compressor during the rolling trials. Firstly, material pre–compression is conducted in the same direction as mill compression. Considering the results of the flat platen confined uniaxial trials, it is evident that such compression produces a significant variance in local sample density within the material blanket. Hence, the local initial properties of the sample are unknown. Secondly, the width of the pre–compressor is 10mm less than the 230mm wide rolls. Hence, despite efforts to bias the placement of the blankets to the viewing side of the mill feeder, the samples did not always mate with the glass window. This resulted in larger fibres often causing shadows on the sample surface; and, more significantly, the prepared cane samples failing to produce a juice film between the glass and the sample over the viewing area, as shown in Figure 5.7.

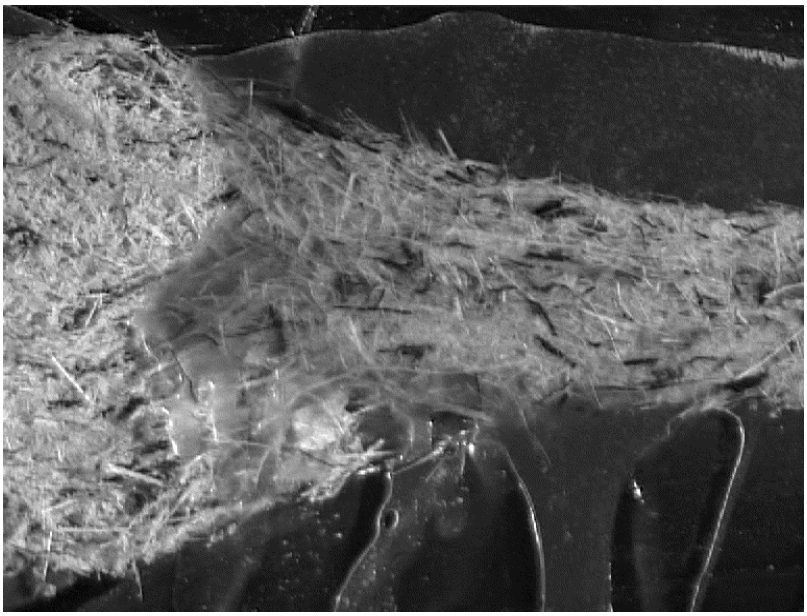

Figure 5.7. Example of juice film failing to occur over entire viewing area.

Furthermore, the reduced sample width allowed free expansion on the opposite side of the blanket, causing a 'folding' phenomenon at the viewing side of the samples as illustrated in Figure 5.8.

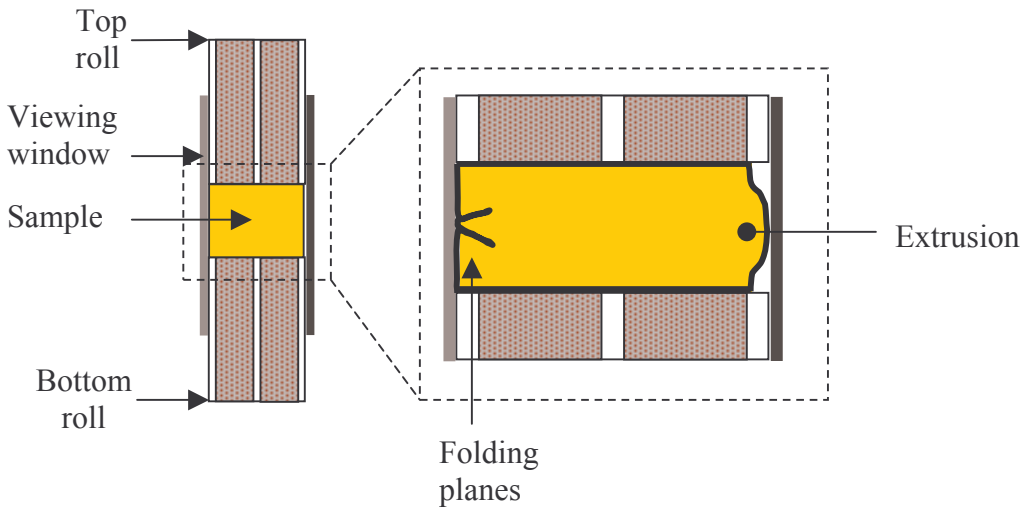

Figure 5.8. Material folding and extrusion due to reduced blanket width.

Finally, the pre–compressor device produced material samples with a parallelogram cross section, such that the visible face of the sample was not vertical. This further reduced the ability to obtain quality mating of the sample with the viewing plane.

5.4.2 Roll fluid drives

The rolls on the experimental milling facility are driven by hydraulic drives. The drives exhibit poor speed control at roll surface speeds in the acceptable range for image capture at the camera frame rate of 25 frames per second. Not only does the surface speed of each roll vary significantly with load; there are also discrepancies between the surface speeds of the two rolls, resulting in variations in the magnitude of roll torque between the rolls. Hence, kinematic steady state testing conditions were not achievable for the rolling trials. As a result of this, the strain behaviour of different regions within a given sample may vary significantly. Furthermore, at the time the rolling trials were conducted there was no means to log the transient rotational speed of the two rolls during the tests. Without knowledge of the transient roll speeds it is very difficult to assess variations in the strain behaviour across the length of each sample.

The speed control problem not only poses difficulties in assessment of ITA deformation results, it also cause difficulties in attempts to computationally represent such experiments in a finite element model, as necessary inputs and conditions are not known. It is also worth mentioning that clever use of the ITA particle–tracking algorithm provides a means for assessing the transient kinematic conditions during an experiment by determining the transient velocity at fixed locations within the images.

5.4.3 Mill structure

The side–plates on the experimental mill are held in place with small beams that bolt to the plates and to the mill frame. During experimentation these members were noted to flex due to the load exerted on the side–plates during material compression. This flexure produced gaps between the side–plates and the sides of the rolls, resulting in the ability for material to then expand into these gaps and pass through the nip at a height greater than the work opening. An example of this is shown in Figure 5.9.

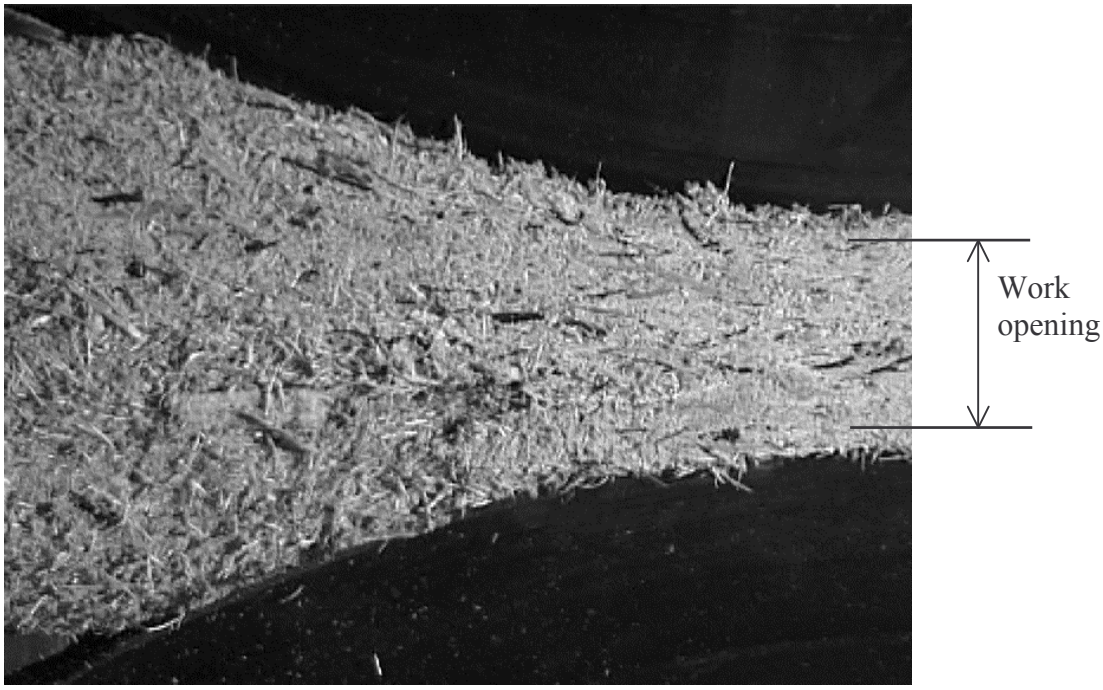

Figure 5.9. Image from a final bagasse test showing the visible height of material exceeding the actual work opening.

Irrespective of the above–mentioned experimental limitations, the rolling trials did provide assessment for the ITA software in regard to measuring the deformation field for the complex two–dimensional rolling regime. However, it is noted that for accuracy in both finite element modelling and ITA deformation mapping of two–roll milling experiments, improved apparatus is required.

5.5 Experimental program

The rolling trials aimed to capture image data over a wide range of compaction for both prepared cane and final bagasse. The experiment was factorial for each of the two materials, involving two nip compactions, two contact angles (or feed heights), and a set of repeats. The target roll surface speed for the tests was set to the minimum of 50 mm/s, in order to obtain small enough incremental fibre displacements for accurate measurement. Information pertaining to the experiments is contained in Table 5.2.

Test	Material	Fibre content	Work opening	Contact angle	Compaction in the nip	Feed height	Sample mass
#	[--]	[dec]	[mm]	[deg]	[kg/m ^{3}]	[mm]	[kg]
1	PC	0.131	40	25	267	110	22.54
2	PC	0.131	40	25	367	110	30.99
3	PC	0.131	40	30	267	140	22.54
4	PC	0.131	40	30	367	140	30.99
5 (1 RPT)	PC	0.131	40	25	267	110	22.54
6 (2 RPT)	PC	0.131	40	25	367	110	30.99
7 (3 RPT)	PC	0.131	40	30	267	140	22.54
8 (4 RPT)	PC	0.131	40	30	367	140	30.99
9	FB	0.523	40	25	400	110	8.44
10	FB	0.523	40	25	550	110	11.61
11	FB	0.523	40	30	400	140	8.44
12	FB	0.523	40	30	550	140	11.61
13 (9 RPT)	FB	0.523	40	25	400	110	8.44
14 (10 RPT)	FB	0.523	40	25	550	110	11.61
15 (11 RPT)	FB	0.523	40	30	400	140	8.44
16 (12 RPT)	FB	0.523	40	30	550	140	11.61

Table 5.2. Rolling trials experimental program.

5.6 Errors in measurement

The load cells on the experimental milling facility were calibrated prior to the experiments, resulting in negligible errors in the measured values of roll loads and torques. The only other notable source of error for the mill is the work opening or minimum distance between the rolls, which was noted to increase with roll load (Kauppila and Loughran 2000). An equation for the work opening deflection in millimetres as a function of load in kilo newtons was developed for the two–roll mill (EQ 5.1).

$$Deflection\ [mm] = (8.9 \times 10^{-3}) \times Roll\ Load[kN] + (0.148) \qquad \text{(EQ 5.1)}$$

Based on the roll load traces from the rolling trials, the maximum error in the work opening can be determined for the two nip compactions used for each material. The work opening deflection and the error in sample mass will result in errors associated with the average nip compactions. These errors are detailed in Table 5.3.

Material	Error in sample mass	Nip compaction	Maximum roll load	Work opening deflection	Maximum error in nip compaction
[-]	[kg]	[kg/m ^{3}]	[kN/Test#]	[mm]	[%]
PC	-0.04	267	21.36/7	0.33	-0.6
PC	-0.04	367	86.91/6	0.92	-2.1
FB	-0.01	400	18.43/11	0.31	-0.8
FB	-0.01	550	93.26/10	0.98	-2.4

Table 5.3. Maximum errors in nip compaction for the rolling trials.

The maximum error in sample compaction is seen to result from the highly compacted samples of each material. The error in average sample nip compaction is low, and natural variations in sample compaction are likely to be large in comparison with the average values. The actual compaction in the nip is also expected to be slightly less than the predicted values, due to extrusion of the material through the mill.

5.7 Experimental results

Video footage taken from each experiment was converted into a Quicktime movie file and stored on the host computer. Each file was decomposed into a sequential series of tiff images for ITA analysis. Load and torque data was recorded for each experiment and stored as Microsoft Excel files.

5.7.1 Mechanical results

The load and torque data for each pair of replicate experiments were plotted against time over the duration of the experiments. The load and torque data plots are contained in Appendix C. Examples of the data are shown in Figures 5.10 and 5.11 for the first pair of prepared cane and final bagasse tests, respectively.

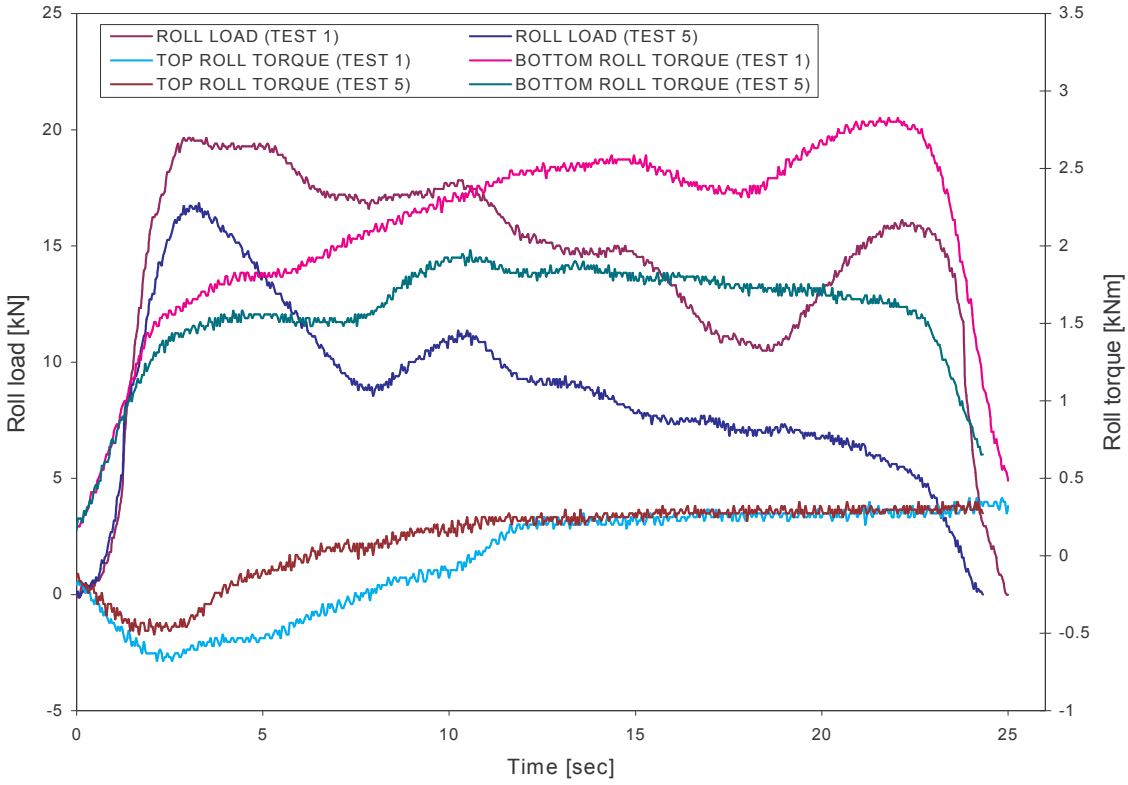

Figure 5.10. Load and torque data for prepared cane: Test 1 and Test 5.

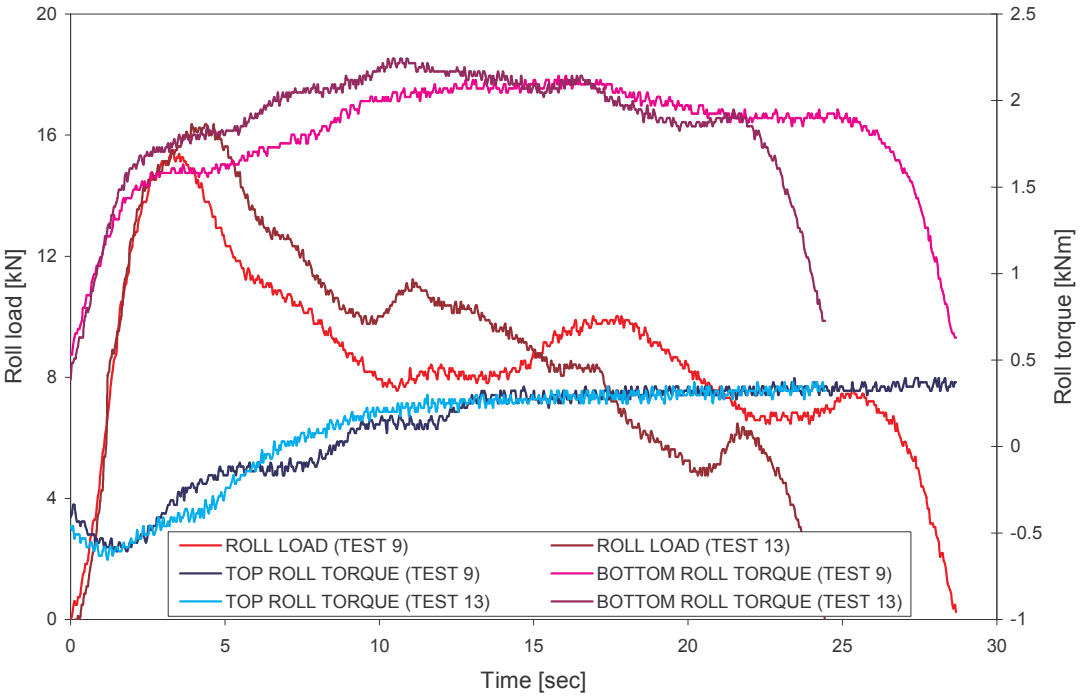

Figure 5.11. Load and torque data for final bagasse: Test 9 and Test 13.

The above figures indicate a definite failure to reach steady state loading conditions due to the inability of the apparatus to maintain constant roll speed under load. The magnitude of the top and bottom roll torques at a given point in time is shown to vary significantly as a result of the speed discrepancies between the two rolls. The repeatability of roll torque was adequate for replicate tests. The repeatability of the roll load was very poor for the replicate experiments. However, it is noted that roll load has previously been documented as a difficult quantity to replicate (Murry 1960) for two–roll milling experiments.

5.7.2 ITA results

Analysis of the rolling trials involved application of the ITA direct software with a three column nodal grid. The position and results for nodes in the centre column of the mesh were stored at each time increment in the analysis for construction of the results domain. The physical size of the camera viewing area and material particles were of similar dimensions to those used in the confined flat platen uniaxial trials. Hence, suitable particle tracking parameters and node spacings were inferred from the results of the sighting trials sensitivity analyses. Based on the average incremental pixel displacement of approximately 7 pixels, a sub–region size of 64 pixels was chosen along with single image time increments (0.04 seconds).

Because the three–column grid only covers a small vertical slice of the sample (approximately 40mm with suitable nodal spacing), many analyses can be conducted for each 1200mm long sample. For the experiments conducted, instabilities in speed load and torque make the choice of which section to analyse very difficult. For controlled experiments, the load would initially peak and then plateau for the remaining duration of the experiment; finally dropping off quickly as the back of the sample passed the nip. In such a situation, analyses would be conducted on the material region corresponding to the period of constant load or steady conditions. Without such conditions, analysis of any two given slices of material (including slices in close proximity to each other) are likely to produce different magnitudes in local deformation results. This problem is unavoidable for ITA analysis of the rolling experiments conducted. None the less, slices of material in the centre region were selected for analysis of the appropriate experiments. It is noted that ITA interpolation software was also developed for application to the two roll milling experiments, involving velocity prediction for points in the fixed grid that lay on the roll surfaces.

This was achieved by determining the theoretical centre and the boundary equation of each roll from two specified image coordinates on each roll boundary. The velocity at some other X, Y pixel location on the rolls could thus be determined by trigonometry and knowledge of the rotational speed of the rolls at the corresponding point in time. However, due to the inability of the milling facility to record the transient rotational speed of the rolls at the time of testing, values can only be assumed. This inevitably leads to inaccuracy in ITA deformation results due to the transient nature of the roll speeds. Hence, deformation results presented for the rolling trials are direct ITA measurements.

5.7.2.1 Prepared cane experiments

The failure to produce a juice film over the viewing area for the prepared cane experiments presented significant difficulties in conducting ITA analysis. The moving juice front thus resulted in incorrect displacement measurements at most nodes in the ITA mesh. Figure 5.12 shows the effect of the moving juice front on the resulting deformed mesh for a transient ITA analysis. The image corresponding to the onset of particle tracking difficulty is also shown in the figure to highlight the sensitivity of the ITA software to such occurrences in testing.

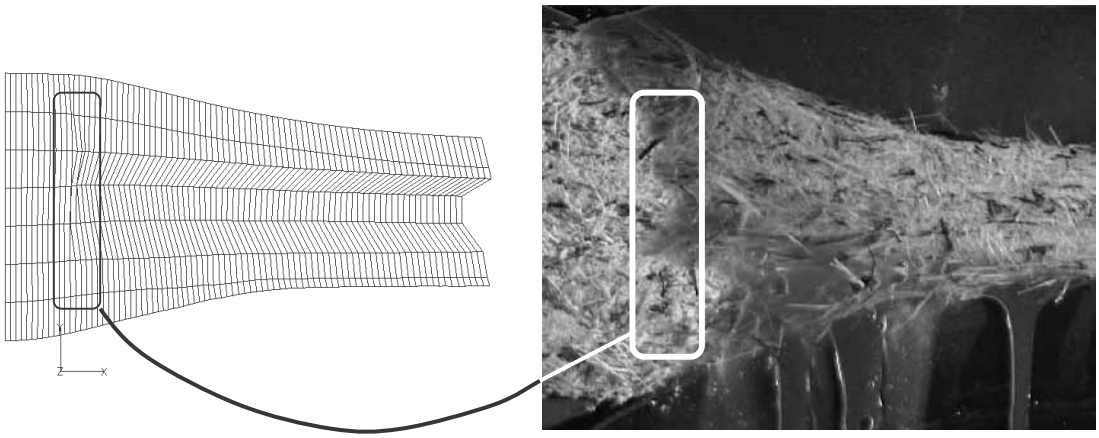

Figure 5.12. Evidence of the difficulty associated with tracking the cane fibre when a moving juice front is present.

Figure 5.12 shows similar particle tracking success in regions that are either free of the surface juice film or completely covered by it, as indicated by the consistent displacements in these two regions of the sample. The particle tracking difficulties result when attempts are made to track particles across the moving front of the juice film.

There were some small sections of footage from the prepared cane tests involving juice coverage of the entire sample viewing area. However, the time over which the complete juice film was present was not long enough for complete transient ITA analysis of a vertical slice of the sample. A single pair of images from one such section of footage was thus used for steady–state ITA analysis of fibre deformation. The main aim of this analysis was to present further evidence that the software is capable of successful image measurement of the prepared cane during rolling, when the juice creates a film over the viewing area. The assumption of steady–state conditions is however invalid, as shown by the mechanical results for the experiments. The deformed mesh is shown in Figure 5.13 for this analysis.

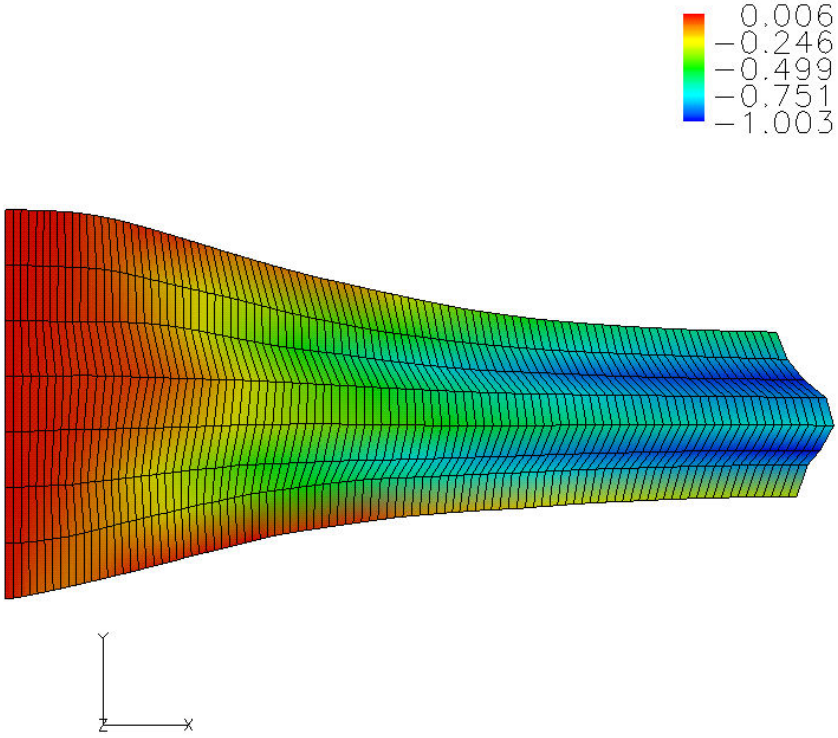

Figure 5.13. Deformed mesh for an ITA steady–state analysis involving a pair of prepared cane images with total sample juice film coverage. The contoured variable is Y–Y Logarithmic strain.

Figure 5.13 shows successful particle tracking for the selected images involving total sample juice film coverage. Incremental displacements corresponded well with manual measurements. The deformed mesh shows an interesting strain distribution across the nip. The strain in the outer regions of the nip is low, as might be expected due to material expanding into the gap between the rolls and the glass window. Inside these outer low strain regions the presence of the roll boundaries is evident in the

form of high vertical and shear deformations. The strain distribution across the 40 mm work opening appears parabolic, with maximum deformations occurring at the roll boundaries and minimum deformations occurring in the centre region of the blanket. The rolls appear to impart high shear on the outer regions of the blanket, causing a folding of the material as it passes through the nip. As a direct result of this shearing behaviour, the centre region of the blanket is seen to pass through the nip prior to the outer regions. This result is certainly interesting when considering Murry's proposal that some material may be passing the axial plane at speeds greater than the roll surface speed (Murry 1960).

ITA steady–state analysis of the prepared cane behaviour provides insight into the mechanisms that govern fibre deformations during rolling. However, without load and kinematic steady–state conditions, quantitative results are isolated because different pairs of images will show varying results, due to the fluctuations in roll speed over the duration of the experiment. Successful transient analysis of the prepared cane tests requires approximately 100 sequential images involving no moving juice front on the sample surface. Unfortunately, the lack of steady–state conditions and sample mating with the viewing window resulted in all the prepared cane tests failing to meet this criterion. Hence, the prepared cane footage was not further analysed.

In order to obtain successful ITA results for samples with high moisture content, specific apparatus is required that uses gravity to advantage by turning the current two–roll arrangement on its side. Thus the viewing window would be level with the ground and gravity would force a juice film over the viewing area of the sample. Furthermore, samples would actually rest on the viewing window, ensuring a quality mate with the glass. Alternatively, an external water source could be used during tests to ensure sample saturation and a constant translucent fluid film over the viewing area.

5.7.2.2 Final bagasse experiments

The problems associated with the large juice volume present in the prepared cane samples were not an issue in analysis of the final bagasse experiments, as no liquid was noticeably extracted (due to the low moisture content of the feed material). ITA results were produced for slices of material in the centre region of each blanket. The deformed meshes for all eight final bagasse tests are shown in Figures 5.14–5.21. The

contoured result shown in all the figures is the Logarithmic strain in the Y direction (Y–Y component of the Logarithmic strain tensor).

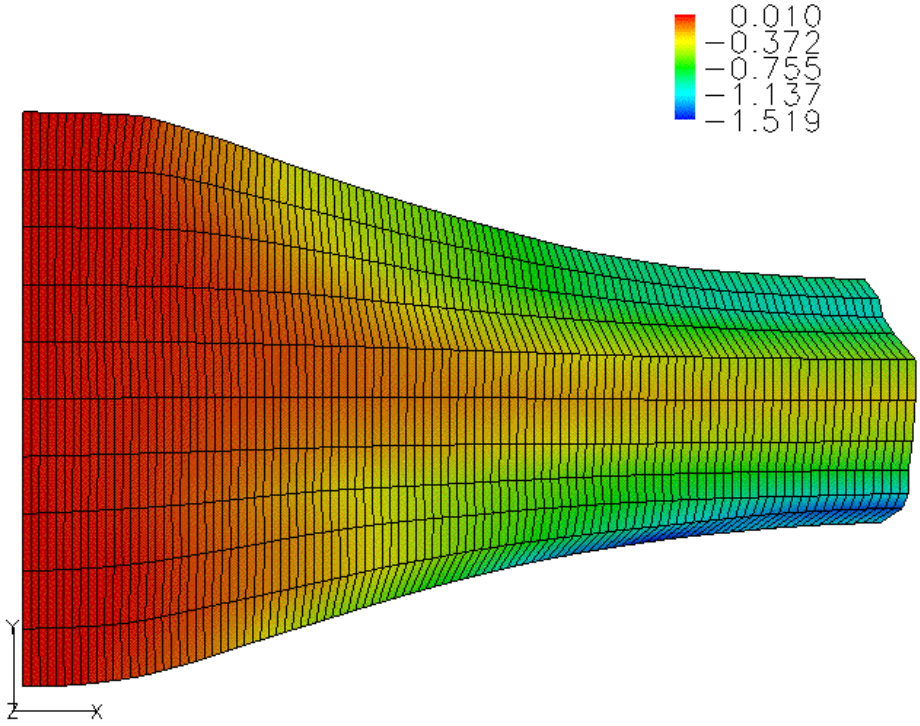

Figure 5.14. Deformed mesh: Test 09, Y-Y Logarithmic strain.

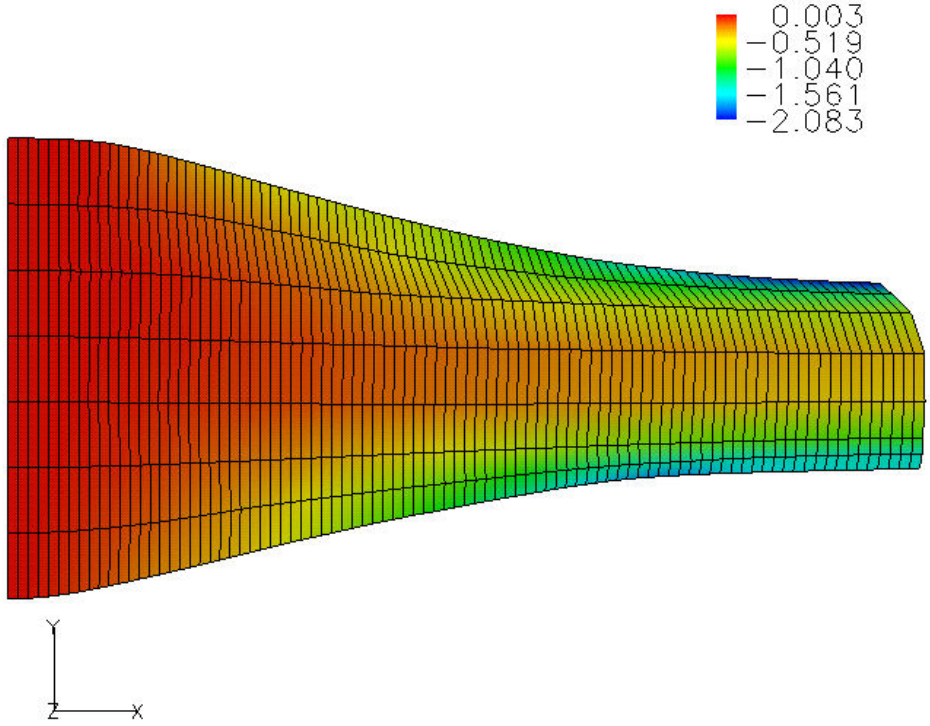

Figure 5.15. Deformed mesh: Test 13, Y-Y Logarithmic strain.

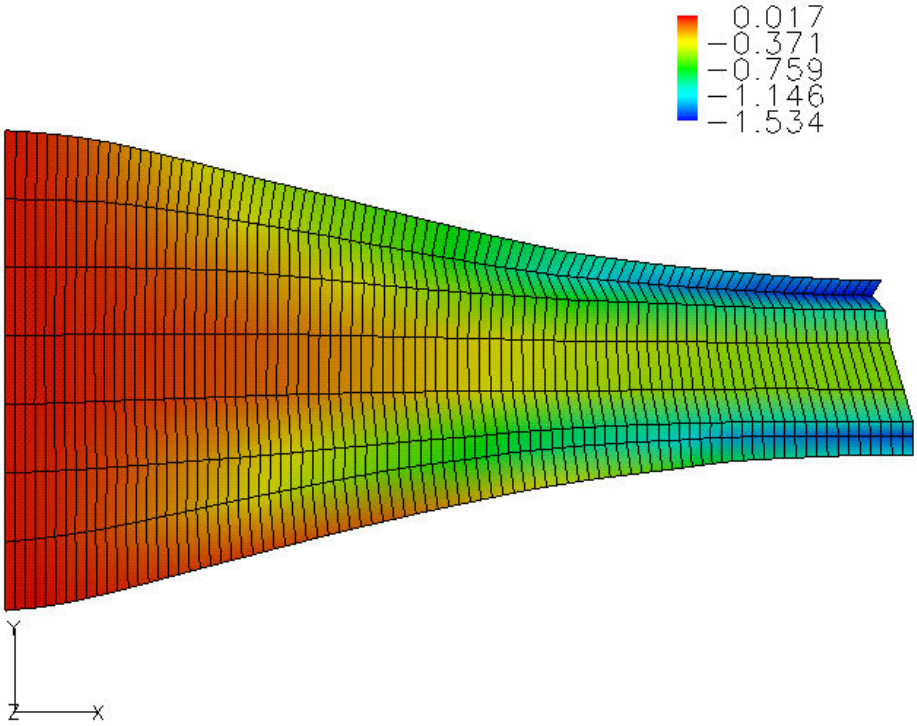

Figure 5.16. Deformed mesh: Test 10, Y-Y Logarithmic strain.

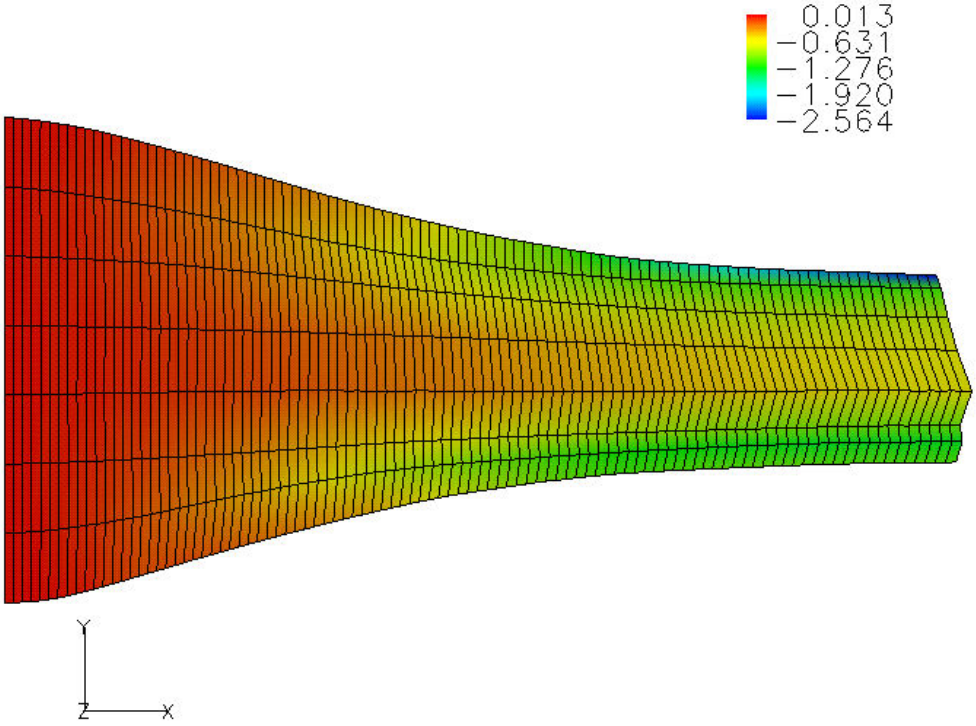

Figure 5.17. Deformed meshes: Test 14, Y-Y Logarithmic strain.

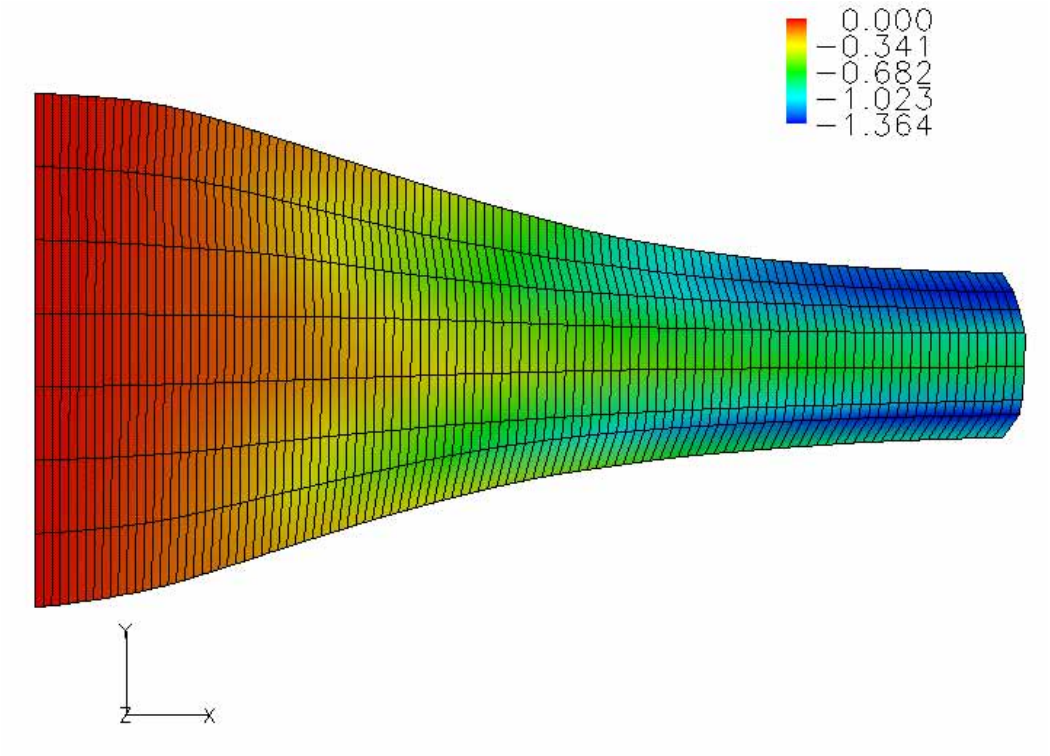

Figure 5.18. Deformed mesh: Test 11, Y-Y Logarithmic strain.

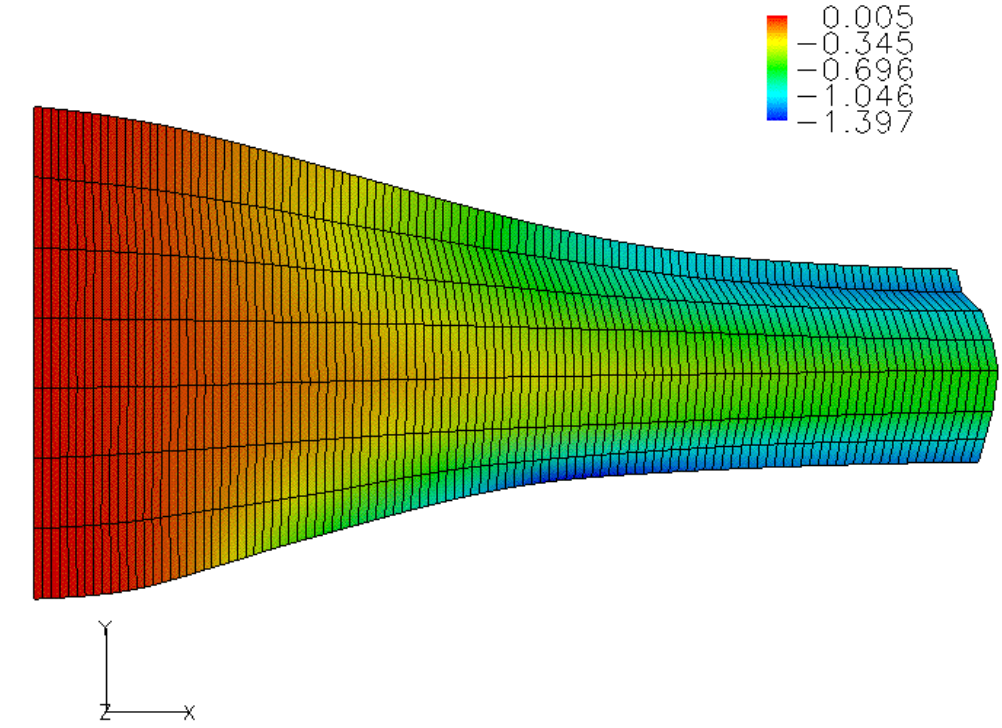

Figure 5.19. Deformed mesh: Test 15, Y-Y Logarithmic strain.

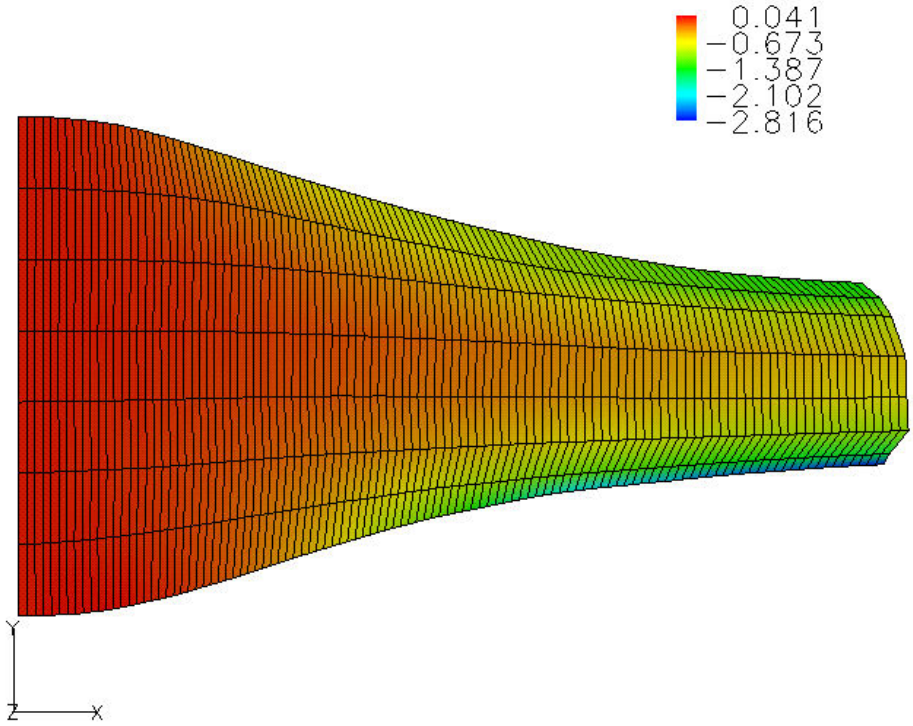

Figure 5.20. Deformed mesh: Test 12, Y-Y Logarithmic strain.

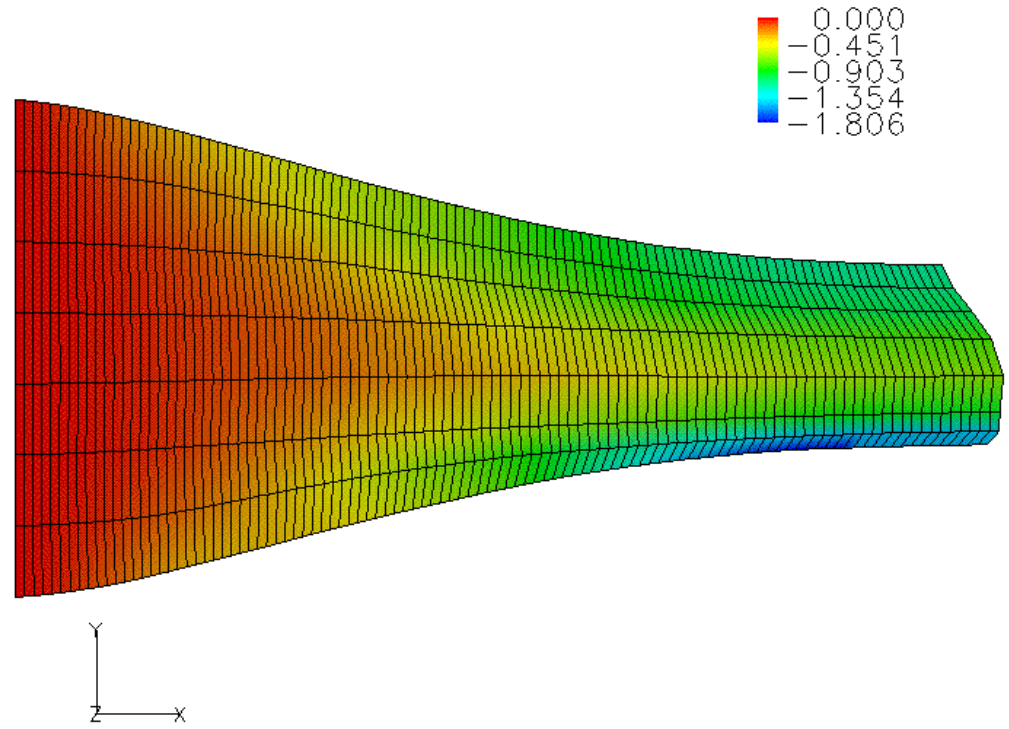

Figure 5.21. Deformed mesh: Test 16, Y-Y Logarithmic strain.

The deformations display strong qualitative trends in strain across the nip. As was seen in the one–off prepared cane steady state analysis, the magnitude of strain in the nip is maximum at the roll surface boundaries and minimum in the centre region of

the blanket. Shearing of the material by the rolls is prominent, resulting in the centre region of the vertical slice passing through the nip prior to the outer regions. There is also evidence of material expansion into gaps between the roll and glass surfaces, in the form of low strain in the material overlapping the roll surfaces. These gaps are a direct result of structural deflection of the side–plate supports under load. The Y–Y Logarithmic strain results across the work opening were plotted and are shown in Figure 5.22.

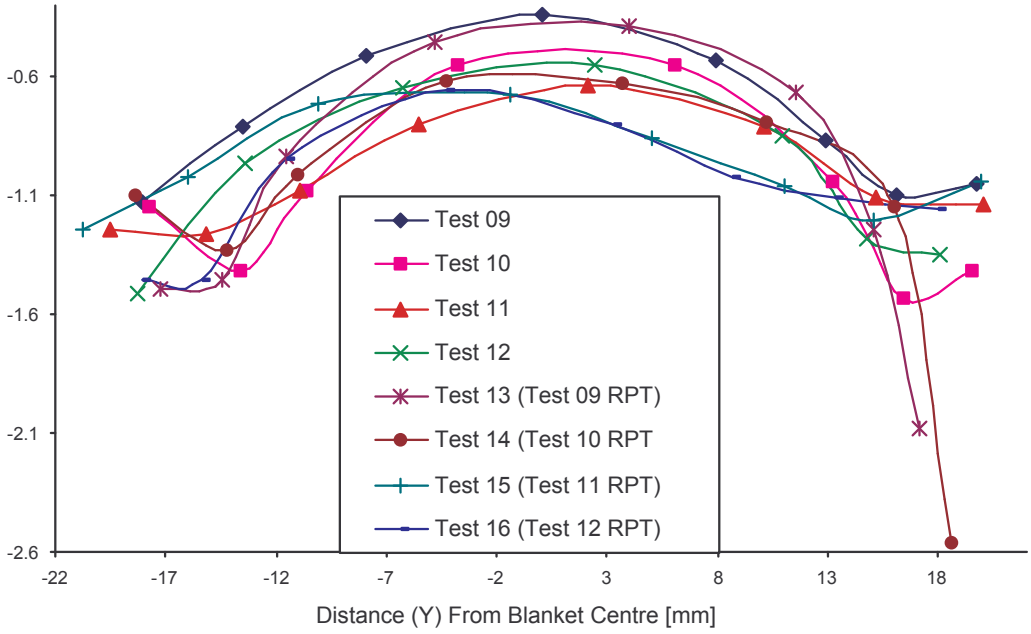

Figure 5.22. Graph showing the Y–Y Logarithmic strain across the work opening for the eight final bagasse tests.

Figure 5.22 shows a somewhat parabolic trend in the magnitude of strain across the nip for the final bagasse analyses. The repeatability of the results for the replicate tests is qualitatively sound. However, it is difficult to make a quantitative assessment of trends in local strain results across the testing parameters such as nip compaction and contact angle. The combination of the pre–compression technique and the folding of the material away from the glass causes localised collapse of visible material and very high local deformations in the two dimensional viewing plane. Thus the range of strain for the tests varies significantly across the tests. In order to make a more representative comparison of deformation in the nip across the experimental

parameters, the average of the Y–Y Logarithmic strain in the nip was determined for each of the above mappings. The resulting values are shown in Table 5.4.

Test #	Contact angle [deg]	Compaction in the nip [kg/m ^{3}]	Feed height [mm]	Sample mass [kg]	Average Y-Y Log strain in the nip [-]
9	25	400	110	8.44	-0.77
10	25	550	110	11.61	-0.79
11	30	400	140	8.44	-0.93
12	30	550	140	11.61	-0.93
13 (9 RPT)	25	400	110	8.44	-0.77
14 (10 RPT)	25	550	110	11.61	-0.78
15 (11 RPT)	30	400	140	8.44	-0.98
16 (12 RPT)	30	550	140	11.61	-0.97

Table 5.4. Average Y-Y Logarithmic strain in the nip for the eight final bagasse tests.

The average strain in the nip is seen to increase in proportion to the contact angle and thus the blanket feed height. In fact the percentage increase in the average strain corresponds well with the 27% (30mm) increase blanket feed height, as may be expected based on overall geometric strains. There is no significant influence of sample mass on the average Y–Y Logarithmic strain in the nip for the final bagasse tests. There is strong repeatability of this average strain result for the replicate tests.

The deformation mapping for Test 11 was selected as a platform for display of further ITA results. The deformation state of the two–roll milling samples is biaxial or truly two–dimensional. Hence the horizontal (X–X) and shear (X–Y) components of the Logarithmic strain tensors will be of notable magnitude. The deformed mesh for Test 11 is shown in Figures 5.23–5.24, contoured with the X–X and X–Y components of the Logarithmic strain tensor, respectively.

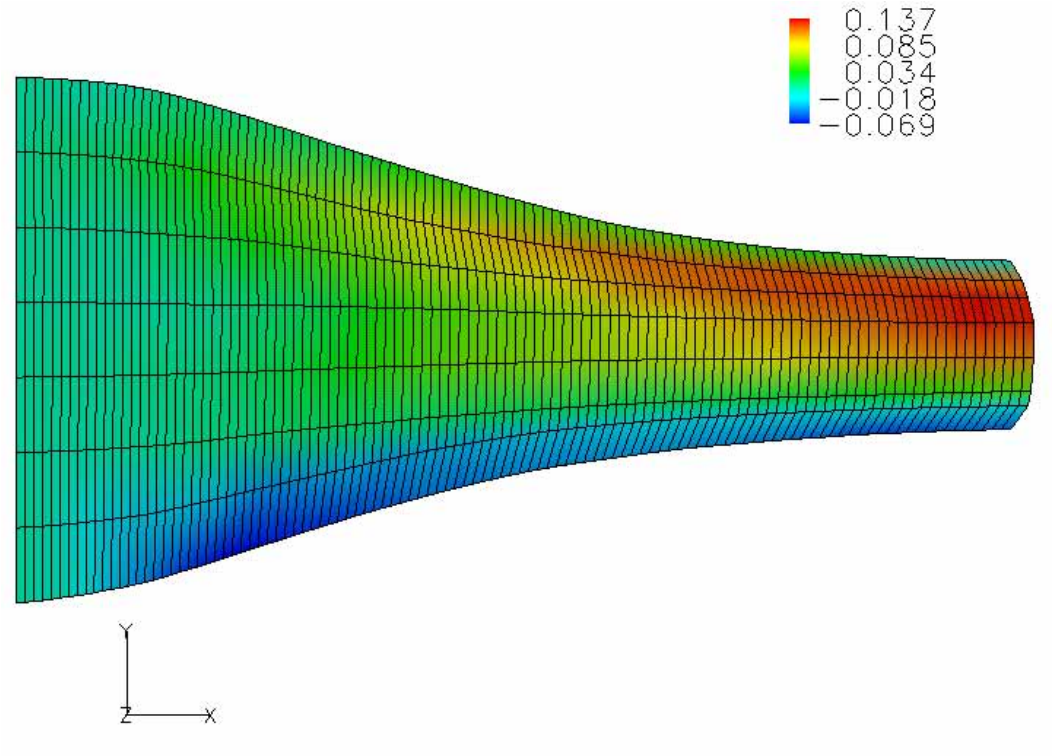

Figure 5.23. Test 11 deformed mesh: Logarithmic (X–X) strain.

Due to the geometric configuration of the feeder and rolls on the milling facility, samples interact with the bottom roll prior to the top roll. This is obviously a limitation in regard to obtaining symmetry in results. Interestingly, the X–X Logarithmic strain contour shows this interaction, in the form of compressive X–X strain in the material as it encounters the bottom roll prior to the top roll. Furthermore, as compression from the rolls increases towards the nip there is a large region of tensile X–X strain or material lateral extrusion through the nip. This tensile region is biased toward the top roll, indicating some rotation of material due to speed discrepancies between the rolls.

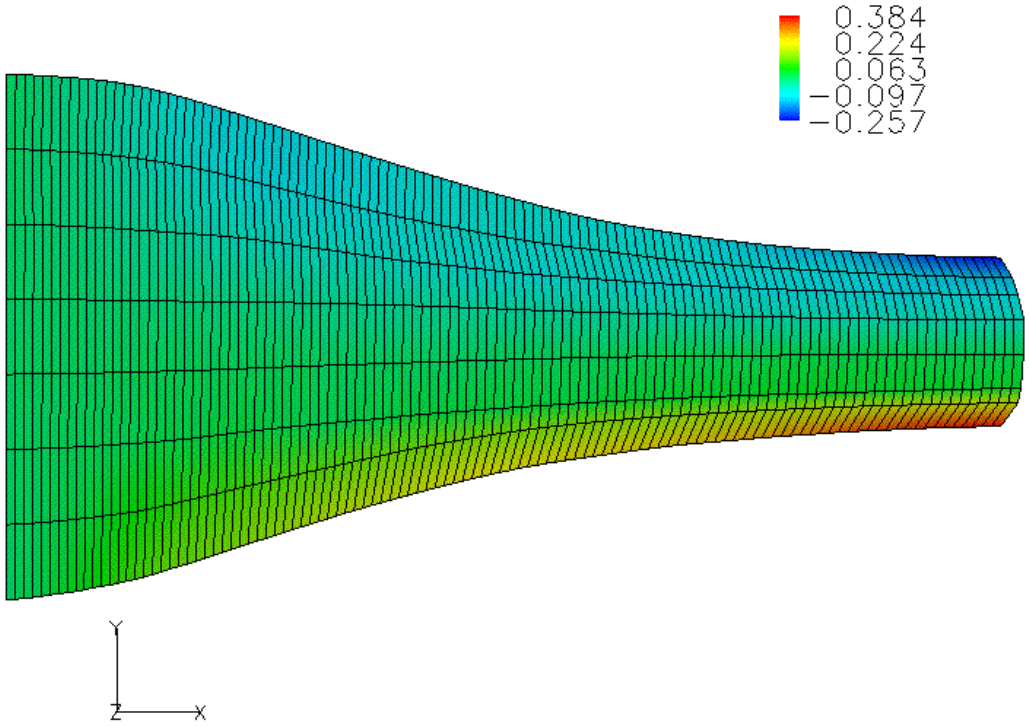

Figure 5.24. Test 11 deformed mesh: Logarithmic (X–Y) shear strain.

The shear strain contour shows positive and negative shear strains in the lower and upper regions of the blanket, respectively. The magnitude of the shear strain caused by the bottom roll is somewhat larger than for the top roll, as might be expected due to the longer interaction of material with the bottom roll.

The Logarithmic volumetric strain is a useful measure of overall deformation for biaxial strain states. The volumetric strain results for the ITA analysis are shown in Figure 5.25.

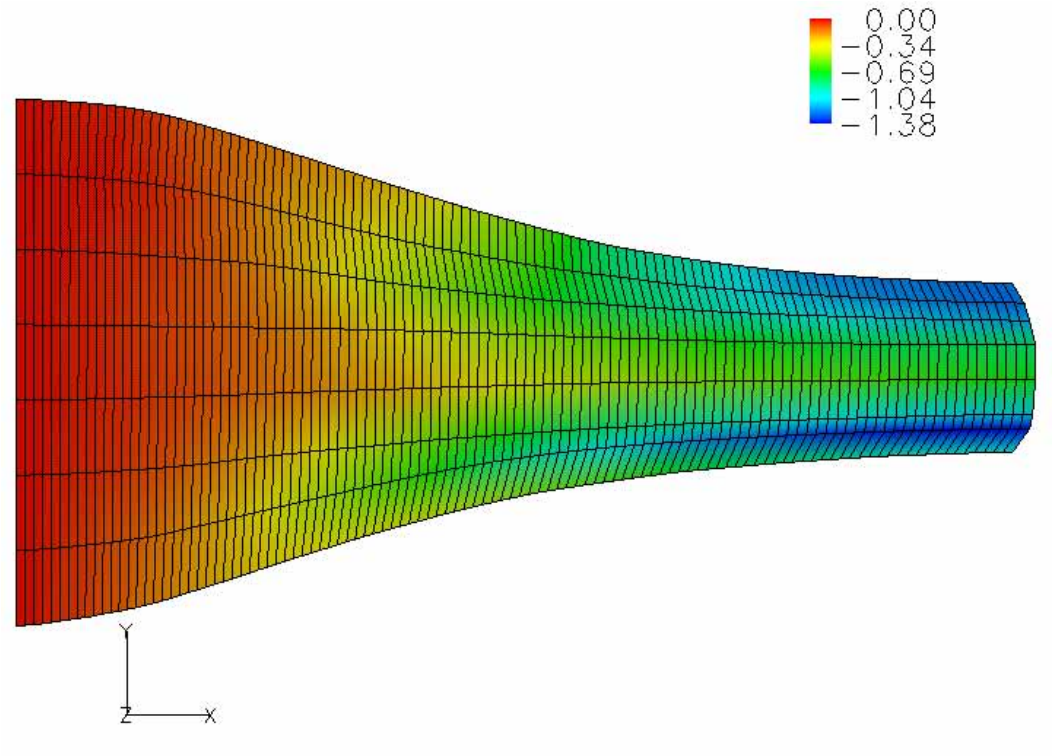

Figure 5.25. Test 11 deformed mesh: Logarithmic volumetric strain.

The Logarithmic volumetric strain results are very similar to the Y-Y Logarithmic strain results, indicating that the deformation state is dominated by the vertical roll compression.

Because ITA outputs the local nodal velocities at each time increment, a comparison with the volumetric theory for material velocity can be made. Volumetric theory assumes that the horizontal material velocity is equal to the horizontal component of the roll surface velocity multiplied by the cosine of the corresponding contact angle (Murry 1960). Based on this theory, material should pass the axial plane (zero contact angle) at the roll surface speed. The target roll surface speed for all tests was 50 mm/s and the contact angle for Test 11 was 30°. This results in theoretical horizontal material velocities in the range of 43–50 mm/s. Figure 5.26 shows the ITA deformed mesh for Test 11 contoured with nodal X velocity in mm/s.

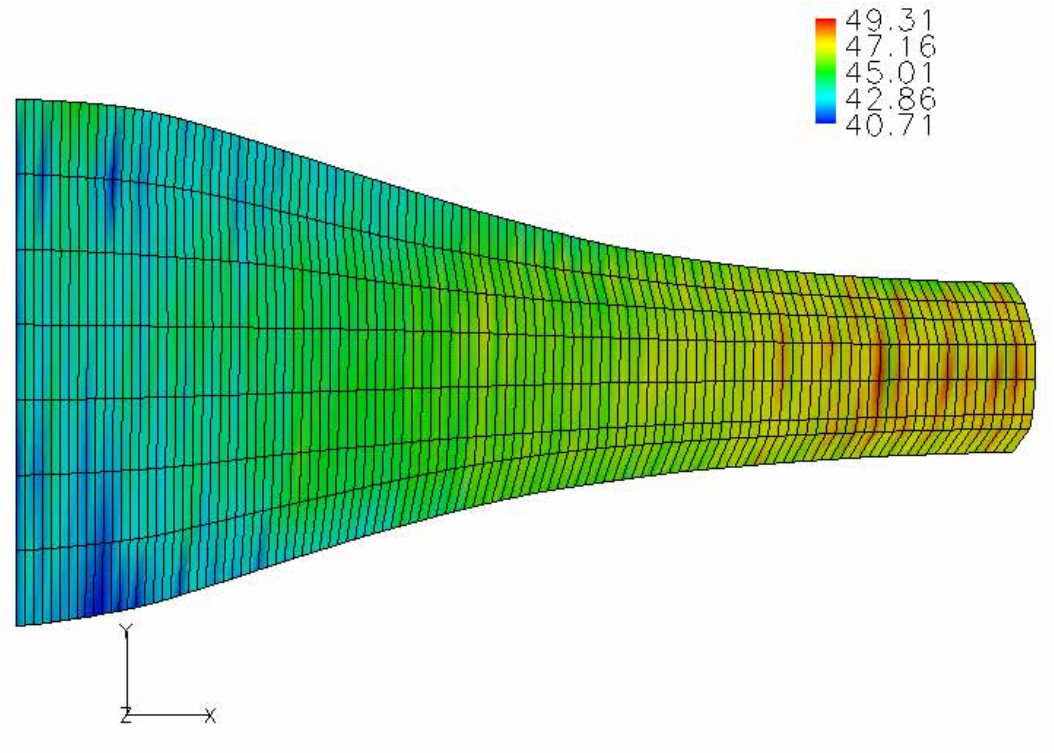

Figure 5.26. Test 11 deformed mesh: Material X velocity [mm/s].

The ITA measured velocities across the domain compare well with volumetric theory, showing velocity to increase with decreasing contact angle. Material is shown to pass the minimum opening (zero contact angle) at close to the target roll surface speed for the slice of bagasse analysed. Unfortunately, the actual surface speed of the rolls was not known at any given time. Thus, it is not possible to directly validate Murry's hypothesis that some material passes the axial plane at a velocity greater than the roll surface speed. However, the extruded profile of the material in the nip indicates that during the compression, the centre region of the blanket is accelerated forward in a folding motion, resulting in the blanket centre passing the axial plane prior to the material at the roll surface.

Making the assumption that the initial material properties are uniform across the sample, updated nodal material data can be determined at each time increment, based on the volumetric deformation at each node. The ITA software calculates a variety of material properties such as compaction, porosity and void ratio. The fibre compaction results for the Test 11 analysis are displayed in Figure 5.27.

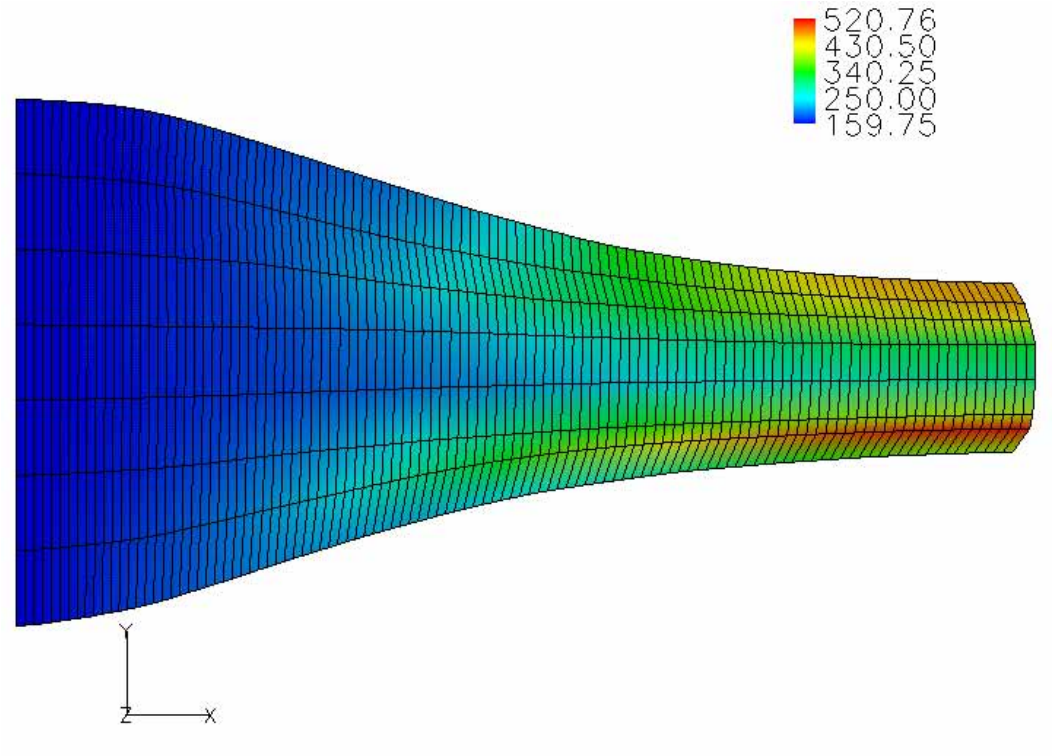

Figure 5.27. Test 11 deformed mesh: Material compaction [kg/m^3].

The compaction in the nip varies in accordance with the volumetric strain. The average measured compaction of material in the nip was determined to be 394 kg/m^3 and corresponds well with the theoretical nip compaction of 400 kg/m^3 for Test 11. Hence, the results show overall conservation of mass for the ITA analysis, despite large variations in local compaction across the work opening.

5.8 Summary

A series of two–roll milling experiments were conducted, involving both prepared cane and final mill bagasse. The rolls were flat and roughened with 60 grit sand paper to enhance surface friction. The experiment was factorial for each of the two materials, and involved two nip compactions, two contact angles and a replicate set of tests. Significant limitations associated with the available apparatus were identified during the trials. Sample geometry and deflection of the side–plate mounts resulted in failure to obtain a quality mate between the viewing window and the sample surface. This scenario caused problems for the prepared cane experiments, as a juice film over the viewing area was not always obtained. Rather, the juice excreted from the fibrous blanket formed a moving front that caused inaccurate fibre displacement measurements. However, small sections of the footage captured for the prepared cane

experiments were identified as suitable for steady–state ITA analysis, and it was shown that complete juice film coverage of the viewing area resulted in accurate ITA measurements for prepared cane.

The final bagasse tests were not influenced by the juice front problem, due to the low moisture content of this material. The time series of images for the eight final bagasse tests were analysed using the ITA software for a section of material in the centre region of each sample. The results showed strong qualitative trends in the measured fields of deformation across the set of experiments, and interesting observations were made, including the obvious presence of forward folding of material through the nip. This folding results in the centre region of the blanket passing the axial plane, prior to material near the roll surfaces.

The Y–Y Logarithmic strain across the nip was shown to have a parabolic profile, with high deformation near the roll boundaries and low deformation in the blanket centre region. However, quantitatively, these results varied significantly due to poor control of the mill roll speeds. The average of measured Y–Y Logarithmic strain in the nip was determined for each test and this quantity was shown to be repeatable for the replicate experiments.

A single analysis was selected for display and discussion of other measured quantities, including lateral, shear and volumetric strains, nodal velocities and fibre compaction. Lateral extrusion of material through the nip was identified in the form of tensile X–X strains of notable magnitude. The measured nodal velocities were shown to correspond with volumetric theory across the domain. The average of predicted nodal compactions in the nip corresponded well with the theoretical average, indicating overall conservation of mass for the ITA predictions.

CHAPTER 6
CONCLUSIONS AND RECOMMENDATIONS

The application of computational mechanics to the numerical modelling of industrial processes is becoming a widely accepted tool for predicting material behaviour and process power requirements. Often, the physical nature of the process material is complex, and engineering assumptions must be made to simplify the material and/or process, for application of available modelling techniques. As a result of these simplifications, the computational model output requires validation from experiment, to consolidate the underlying model assumptions.

The use of appropriate experimental methods and data logging equipment provides a valuable means for validation of mechanical model output such as reaction forces and moments. However, the lack of measured local material kinematics, often presents difficulties for validating the predicted physical behaviour.

Over the past decade in Australia, there has been a significant research drive towards the successful constitutive modelling of the sugar milling process materials, prepared sugar cane and bagasse. In order to achieve this goal, a better understanding of the physical behaviour of the solid–phase fibre is required. The accurate measurement of the fibre blanket kinematics was identified as a novel means for validating computational model output, and for gaining an improved understanding of material behaviour during the milling process. Furthermore, accurate measurement of experimental fibre deformation fields, coupled with experimental mechanical output, presents the possibility of parameter refinement within the solid–phase material model.

This chapter revisits the achievements and salient findings of this doctoral investigation. Recommendations are also made, in regard to future numerical and experimental investigation into accurate image measurement of bagasse kinematics.

6.1 Conclusions

This study has succeeded in applying numerical image displacement measurement and fundamental continuum mechanics, to the direct measurement of two–dimensional finite fibre strains, from digital images taken of prepared cane and bagasse experiments.

6.1.1 The image processing system

Visualisation of uniaxial compression and two–roll milling experiments was achieved via an inexpensive image acquisition system. To make the appropriate material surfaces available, viewing windows were designed and fitted to uniaxial test cells and to the C.R. Murry two–roll milling facility. Positioning the camera axis orthogonal to the desired viewing plane was identified as crucial for image measurement accuracy. Hence, a precision traversing system was designed and manufactured, that allowed the camera position to be adjusted for different tests, without disturbing its orthogonal position to the viewing plane. Light shrouds were also employed to improve the image quality, by eliminating the reflection from the surrounding environment. The material surface was illuminated using incident light from a two–thousand Watt quartz tungsten halogen studio lamp. Sequential images were captured and digitised via a SONY 3-CCD digital video camera with a frame rate of 25 frames per second and built–in frame grabbing hardware. Image storage and treatment was achieved using an Apple I-mac host computer.

A generic image analysis tool (ITA) was developed for measuring two–dimensional finite strain material kinematics, from time series of digital images. The ITA software combines the theories of image displacement measurement using the FFT direct cross–correlation method, and fundamental continuum mechanics, to present kinematic output concurrent with finite element models. The (ITA) software was constructed in FORTRAN syntax.

To map the two–dimensional transient motion of a desired material surface, a direct particle–tracking algorithm was implemented to follow each node in a rectangular grid, through the time series of digital images. This was achieved by employing the FFT direct cross–correlation theorem, to measure the average pixel displacement of an image sub–region surrounding each node, between each pair of sequential images in the series.

The deformation gradient tensor, consisting of the spatial gradients of the material motion, is of fundamental importance for calculation of the material deformation tensors and the desired modes of finite–strain tensors. Hence, for the ITA software to be a generic image analysis tool for measuring Lagrangian finite material strains, a suitable means for approximating the spatial gradients across the deformed grid was required. Second order point difference operators were employed to approximate the

four partial derivatives of each nodal position with respect to its initial position in the grid.

Calculation of the deformation gradient infers the underlying assumption that material motion is smooth and continually differentiable, and also demands the presence of a defined reference configuration. Following the practices of the finite element mill modelling procedure, and for simplicity, the initial grid location was chosen as the reference configuration for the ITA spatial gradient approximations. Hence, the initial grid poses as the material zero–strain configuration.

Cauchy's polar decomposition theorem was used to determine the right and left stretch and Cauchy–Green deformation tensors. The Green–Lagrange and Logarithmic strain tensors were identified as the most suitable measures of large finite strain for making direct comparisons between measured (ITA) and predicted (finite element model) material strains. Principal and volumetric strains were also evaluated for each of the strain tensors.

To make the deformation results available at all times in the analysis, the four components of the deformation gradient, stretch and various Lagrangian strain tensors, were calculated for all times in the analysis. Due to the relatively low computational cost of the point difference calculations compared to the FFT displacement measurements, this decision caused no noticeable increase in solution time for a given ITA analysis.

The time rate tensors (deformation rate, rate of strain and spin) were identified as important quantities for assessment of process conditions. The deformation rate tensor was determined for each node, using second order point difference operators to measure the change in each component of the deformation gradient with time. The velocity gradient was evaluated and decomposed into its symmetric (strain rate) and antisymmetric (spin) parts. These quantities were also calculated at all available times in the analysis.

Nodal material outputs, such as local void ratio, compaction and compression ratio were also identified as important output for this application of the ITA software. The assumption of non–deformable fibres was made, such that material parameters could be evaluated via knowledge of the initial sample mass, volume and fibre content, and the determinant of the deformation gradient (Jacobian). Without available means (densitometer) for determining the variance in initial local fibre density in the blanket,

the assumption of uniform initial density was made, to allow the update of material parameters throughout the analysis.

The ITA results were output in various formats, to allow various levels of post–processing. Selected nodal outputs were stored in a simple binary data file, for use in software packages such as Microsoft Excel© and S–Plus©. Nodal positions, and ninety–seven other chosen ITA scalar and vector quantities were stored in grid and results files respectively, for data visualisation using the software package Fieldview©. A customised data reader was written within the Fieldview software, for successful interpretation of the ITA data files.

The ITA software was initially created for the continuous milling process, and involved only a three–column grid that covered a vertical slice of the experiment sample. Confined flat–platen uniaxial compression was identified as an ideal scenario for calibration of the ITA software, for the materials in question. Analysis of uniaxial compression required to extension of the three–column rolling grid, to an n–row by m–column grid, for full sample analysis.

In order to obtain image data for assessing the application of the ITA software to prepared cane and bagasse, a small series of confined flat–platen uniaxial compression experiments (sighting trials) was conducted. To assess the degree of ITA measurement accuracy, a factorial numerical experiment was conducted.

Various combinations of time increment between images, and sub–region size, were each tested for displacement accuracy of the ITA measurements, by comparing the final predicted pixel location of the analysis point, with manual measurements taken from the image series using the NIH-Image© viewing software. Certain combinations were identified to produce very accurate results (less than 1% error in total displacement) across the entire sample, thus validating the ITA technique for measuring local material displacements for both prepared cane and bagasse.

The use of suitable mesh density was found to be crucial for obtaining representative deformation results. Suitable node spacing within the ITA grid was determined via testing over a wide range of node spacings (3–45 mm), and assessing the predicted deformation as a function of node spacing. Node spacings in the range of 25–35 mm were identified to produce the optimal deformation results.

Preliminary ITA analyses of the sighting trials image data identified the need for smoothing nodal abnormalities within the ITA deformed mesh associated with large relative fibre motions locally within samples. An alternative particle–tracking

algorithm was created, involving linear weighted interpolation of nodal displacements, from four surrounding positions in a fixed grid.

The presence of external platen boundaries was also identified to have a significant effect on the accuracy of displacement measurements in the material regions close to these surfaces. As a node approached a platen boundary, the associated sub–region would overlap the platen surface in the image. The platen surface was seen to dominate the displacement measurements, for sub–region overlap greater than about one–quarter of the subregion size. Measurement resolution in material regions approaching the platen boundaries was increased via digital image masking and a sub–region reduction routine, thus allowing nodes to accurately approach these external boundaries.

6.1.2 Confined uniaxial compression experiments

Deformation results from the sighting trials identified the inherent difficulty in obtaining both uniform initial sample density and a 'plane strain' scenario for the simple confined uniaxial compression regime. The ITA deformation mappings of the samples showed large variance in strain with no distinctive trend in the direction of compression, as might be expected due to cell wall friction. This behaviour was attributed primarily to sample loading, and pre–compression in the same direction as the experiment compression. Furthermore, the presence of large material particles within samples of both materials was hypothesised to contribute to the erratic nature of the local material motion during compression. The large particles were seen to reorient during consolidation, resulting in large local strains and collapse of the grid during the compression. The need for repetitive experiments was also identified as a means to assess the repeatability of measured deformations.

The uniaxial cell depth was reduced from 98 mm to 25 mm in order to restrict material motion perpendicular to the two–dimensional viewing plane, thus more closely approaching a plane–strain scenario. A new method involving loading the samples into the cell and pre–compressing perpendicular to the direction of the experiment compression was implemented; with the aim to achieve more uniform initial sample density.

A fines material was manufactured by sieving the finer particles from final bagasse, with a view to showing a reduction in deformation variance with the exclusion of the larger particles.

The auxiliary trials were thus conducted with the above testing modifications in place. Deformation results for final bagasse showed a repeatable trend in deformation in the direction of compression. The strain was seen to vary linearly in the direction of compression, with high strain near the moving platen, and low strain at the stationary platen; as might be expected due to cell side wall friction. Local variations in the deformation data across the width of the cell were still evident, due to the influence of the larger bagasse particles within each sample.

The deformation results for the fines material showed a similar, yet stronger trend in deformation in the direction of compression. Variations in the strain across the sample width were significantly reduced with the omittance of the larger bagasse particles, hence proving their contribution to variance in sample deformations.

A single test was also conducted using the coarse bagasse fibres that were omitted to produce the fines material. ITA analysis of this experiment showed large variations in local deformation, providing further validation of the large fibre hypothesis.

The cell and sample loading modifications significantly improved the initial sample homogeneity and the planar nature of the sample strain. However, for a material such as final bagasse, the presence of a large fibre size distribution infers an inherent difficulty in obtaining plane–strain conditions.

The ITA results from the auxiliary trials are certainly suitable for validation of finite element deformation results for the situation of confined flat–platen uniaxial compression. However, it is noted that for this simple one–dimensional loading scenario, is not difficult to match experimental loads using critical–state material theory.

The ancillary application of the image acquisition system and ITA software to determining the failure modes of prepared cane and bagasse blankets during compression between grooved–platens, was also presented, identifying the role played by the ITA software in this investigation.

Time calibration of the video and load/displacement data provided a means for assessing the mode and severity of the blanket failures, as well as the load required to cause them. Qualitative assessment of the bagasse behaviour during grooved–platen compression, identified the inefficiencies of roll grooves, despite their requirement for mill feeding.

The ITA software was applied to the digital imagery from selected grooving experiments. In most cases, the large displacements applied to the samples, combined

with the small viewing area and the discrete nature of the material/groove interactions, caused excessive local mesh distortions. Hence, nodal singularities in the ITA results were observed. However, qualitatively, the results provided significant insight into the development of pressure within the blanket, via animation of the fibre strain field.

The results indicated that saturation initiates at the groove tips, with juice initially flowing into the low–pressure region of the groove void, or back into the sample. Then, as overall sample deformation increases, the juice is forced out of the sample through the low–pressure material in the grooves, exiting into the groove until the applied compression ceases. It is noted that the low-pressure regions of material present in the grooves provide paths of low resistance for juice flow through the nip, and are hence likely to contribute to reabsorption.

6.1.3 Two–roll milling experiments

A series of two–roll milling experiments were conducted, involving both prepared cane and final mill bagasse. The rolls were flat and roughened with 60 grit sand paper to enhance surface friction. The experiment was factorial for each of the two materials, and involved two nip compactions, two contact angles and a replicate set of tests.

Significant limitations associated with the available apparatus were identified during the trials. Sample geometry and deflection of the side–plate mounts resulted in failure to obtain a quality mate between the viewing window and the sample surface. This scenario caused problems for the prepared cane experiments, as a juice film over the viewing area was not always obtained. Instead, the juice excreted from the fibrous blanket formed a moving front that caused inaccurate fibre displacement measurements.

However, small sections of the footage captured for the prepared cane experiments were identified as suitable for steady–state ITA analysis, and it was shown that complete juice film coverage of the viewing area resulted in accurate ITA measurements for prepared cane.

Material in the centre of the blanket was seen to accelerate through the nip in relation to the regions close to the roll surfaces. This measured forward–folding behaviour of the fibre blanket indicates that the rolls cause internal shearing within the blanket,

resulting in the material slipping on itself as it enters the nip, and the centre region passing the axial plane, prior to the material at the roll surfaces.

The final bagasse tests were not influenced by the juice front problem, due to the low moisture content of this material. The time series of images for the eight final bagasse tests were analysed using the ITA software for a section of material in the centre region of each sample.

The results showed strong qualitative trends in the measured fields of deformation across the set of experiments. The Y–Y and volumetric Logarithmic strains across the nip was shown to have a parabolic profile, with high deformation near the roll boundaries and low deformation in the blanket centre region. The similar magnitudes of these two quantities confirmed the belief that two–roll milling was significantly dominated by the vertical compression. The average of measured Y–Y Logarithmic strain in the nip was determined for each test and this quantity was shown to be repeatable for the replicate experiments.

Varying magnitudes of forward–folding of the fibre blanket were measured for all eight experiments. This measured behaviour consolidates Murry's theory, that material passing the axial plane at a speed greater than the roll surface was a major contributor to measured excess bagasse volume rates, and to reabsorption. With the lack of roll speed data logging, it was not possible to know the actual roll speed during the ITA analyses. Hence, qualitative validation that the material was travelling faster than the roll was not achievable for the tests. However, assuming that the material at the roll surface was travelling at the roll speed, this was evidently the case.

A single analysis was selected for display and discussion of other measured quantities, including lateral, shear and volumetric strains, nodal velocities and fibre compaction. Lateral extrusion of material through the nip was identified in the form of tensile X–X strains of notable magnitude. The measured nodal velocities were shown to correspond with volumetric theory across the domain. The velocity contour plot gave further indication that the rolls slowed the adjacent material, thus imparting internal shear within the blanket, resulting in the forward acceleration of the blanket centre region.

The average of predicted nodal compactions in the nip corresponded well with the theoretical average, indicating overall conservation of mass for the ITA rolling predictions.

6.2 Recommendations

This study presents the first application of numerical image displacement measurement to determining the local kinematic behaviour of prepared cane and bagasse. Significant advancements were made in regard to both creating an appropriate numerical tool, and application of this tool for measurement of local bagasse deformations. There are however, many avenues for further study in this area.

6.2.1 Image analysis

This investigation has dealt with the treatment and displacement measurement of raw digital images, taken from suitable experiments. The software tool developed was shown to be capable of measuring large material strains, with a high level of accuracy. However, further work is required in order to determine whether or not post–capture image manipulations (threshold, sharpen etc.) can improve the measurement accuracy further. Such an investigation is not considered crucial at this stage, as this investigation has shown acceptable measurement accuracy for application to raw grey–scale images of both prepared cane and bagasse.

Experimental modifications and further testing are currently considered more important for research progress, in order to obtain more representative measurements of both rolling and grooving deformation states.

6.2.2 Confined uniaxial compression experiments

The deformation field associated with plane strain confined flat–platen uniaxial compression has been accurately quantified for bagasse, and also a fines material, via refined experimental practices. Similar experiments involving prepared cane will result in the accurate measurement of this material during this simple loading scenario. Prepared cane is likely to show significant differences in compression behaviour, due the presence of liquid and increased cohesion. A comparison study between prepared cane and first mill bagasse might allow distinctive separation of fibre deformations caused by external mechanical loads and internal juice loadings.

The implementation of the same experimental procedure, involving grooved–platens, will produce significantly improved measurements of this complex material strain state, for both prepared cane and bagasse. Such measurements will result in a vast improvement in the understanding of both fibre and juice behaviour during the factory

milling process. Furthermore, this complex strain state presents a more critical assessment of the critical state material model used to represent the fibre–phase of bagasse within finite element simulations.

6.2.3 Direct shear experiments

Direct shear tests are crucial for measuring critical–state parameters for the solid–phase material model employed in finite element simulations. The application of the ITA software to footage from direct shear tests, will provide further insight into the critical–state behaviour of bagasse fibre, as well as providing critical assessment of computational simulations for another experimental regime.

6.2.4 Two–roll milling experiments

In order to obtain accurate quantitative ITA deformation measurements for milling, further two–roll experiments are required. Certain apparatus limitations identified in this study have since been corrected, including an improved pre–compressor device, better roll speed control and stronger side–plate mounts. Furthermore, data logging now exists for roll speed, providing important knowledge for assessment of ITA results, as well as allowing the creation of accurate finite element simulations of experiments. Further testing with the C.R. Murry two–roll milling facility will produce improved deformation measurements, allowing validation of two–roll milling finite element simulations. Furthermore, better mill control and performance under load will provide improved measurement of deformation trends across ranges of various milling parameters.

Two alternatives are presented for eliminating the juice front problem associated with the prepared cane experiments. Ideally, the mill configuration would be turned ninety degrees, such that the sample rests on the viewing window, with gravity ensuring juice coverage of the viewing area. However, the current apparatus is not capable of rotation in this direction, hence new apparatus is required in order to achieve such an arrangement. A suitable alternative to a specific rolling apparatus might be to introduce external water to the sample during compression, mechanically ensuring liquid coverage of the viewing area.

6.2.5 Proofing of constitutive material models

Application of the ITA technique to refined material experiments provides kinematic data for direct validation for predicted solid–phase material behaviour within numerical process simulations. ITA results may be used to validate such models at many levels. Firstly, direct comparison of measured and predicted deformations will provide a simple means of assessing the solid–phase model capability, in regard to the numerical prediction of material strain behaviour. Furthermore, ITA data presents the possibility of a reverse finite element solution technique, by forcing the known kinematics on the computational material domain, and solving for material model parameters that will return correct mechanical outputs such as reaction forces and moments.

The application of the ITA software to controlled quasi–static and dynamic process experiments presents a further modelling tool that will allow the assessment of solid–phase constitutive relationships, via Cauchy's laws of continuum mechanics and the Euler–Cauchy stress principle. According to these theories, for quasi–static conditions, the divergence of the stress tensor at all body points (or nodes in the ITA analysis) is zero. Hence, measured quasi–static strain fields from ITA analyses may be used to assess candidate stress–strain relationships based on this zero divergence criteria. Furthermore, application of the ITA technique to controlled dynamic experiments will allow further assessment of these constitutive relationships, via nodal solution of Cauchy's first law using ITA accelerations and nodal densities. Hence, a solution for the finite stress tensor divergence may be found, and constitutive relationships further interrogated in regard to prediction of this finite divergence under complex dynamic rolling conditions.

6.2.6 Three–dimensional ITA

It is noted that the ITA procedure is at this stage limited to two–dimensional plane strain scenarios. Thus, the capability of the technique is limited in regard to describing three–dimensional complex material motions. Further development of the software, coupled with advanced multiple camera systems, active tracer particles or three–dimensional holography methods will see the capabilities of the ITA procedure increase exponentially. However, such apparatus are extremely expensive in comparison to the low cost, highly functional two–dimensional system developed during this study.